Defence Research and Development Canada | Recherche et développement pour la défense Canada

CAN UNCLASSIFIED

DRDC | RDDC
technologysciencetechnologie

Analysis of Seeded Defects in Laser Additive Manufactured 300 M Steel

Dr. Shannon P. Farrell
DRDC – Atlantic Research Centre

Joseph Deering
DRDC – Atlantic Research Centre and
Department of Engineering, Dalhousie University

Journal of Materials Performance and Characterization
Volume 7, No. 1
Pages 300–315
doi:10.1520/MPC20170162

Date of Publication from Ext Publisher: April 2018

Defence Research and Development Canada
External Literature (P)
DRDC-RDDC-2018-P104
July 2018

Canada

IMPORTANT INFORMATIVE STATEMENTS

This document was reviewed for Controlled Goods by Defence Research and Development Canada (DRDC) using the Schedule to the *Defence Production Act*.

Materials Performance and Characterization

doi:10.1520/MPC20170162 / Vol. 7 / No. 1 / 2018 / available online at www.astm.org

Shannon P. Farrell[1] and Joseph Deering[2]

Analysis of Seeded Defects in Laser Additive Manufactured 300M Steel

Reference

Farrell, S. P. and Deering, J., "Analysis of Seeded Defects in Laser Additive Manufactured 300M Steel," *Materials Performance and Characterization*, Vol. 7, No. 1, 2018, pp. 300–315, https://doi.org/10.1520/MPC20170162. ISSN 2379-1365

ABSTRACT

This research activity was initiated to better assess the capacity for traditional nondestructive testing (NDT) approaches to ascertain the defects inherent to materials fabricated through a directed energy laser additive manufacturing (LAM) process. A methodology was developed to intentionally seed defects in 300M steel specimens through intermittent modification of fabrication parameters. Several 300M steel specimens were fabricated and the concentration of defects or bulk density was characterized using optical microscopy and variations of the Archimedes' principle. Specimens were then evaluated using NDT (radiographic testing, ultrasonic testing). Results show that by using n-hexane as the displacement liquid, the Archimedes' principle was found to have repeatability in density values of 0.1 ± 0.1 %. The results reveal the unique defects produced through the LAM process and the limitations for conventional NDT techniques to adequately detect defects in LAM materials. Ultrasonic testing was found to be a promising tool for assessing the LAM defect distribution. Future work will focus on LAM alloys with higher densities and relate microstructure and defects to overall material performance.

Keywords

additive manufacturing, directed energy, selective laser melting, Archimedes' principle, density, defects, porosity, ultrasonic spectroscopy, radiographic testing

Manuscript received November 8, 2017; accepted for publication April 9, 2018; published online July 17, 2018.

[1] Defence Research and Development Canada, 9 Grove St., Dartmouth, Nova Scotia B2Y 3Z7, Canada (Corresponding author), e-mail: shannon.farrell@drdc-rddc.gc.ca, https://orcid.org/0000-0001-7954-9423

[2] Defence Research and Development Canada, 9 Grove St., Dartmouth, Nova Scotia B2Y 3Z7, Canada; and Department of Engineering, Dalhousie University, 5248 Morris St., Halifax, Nova Scotia B3H 4R2, Canada

Introduction

Additive manufacturing (AM) is an emerging disruptive technology that is expected to revolutionize material and product fabrication on a global scale and have an impact on industrial competitiveness and national security. This is primarily due to the inherent flexibility of the fabrication process to produce structures with radical geometries and unique microstructures. The complexity of the fabrication process leads to the safeguarding of the intellectual property by manufactures and developers. Many AM fabrication systems operate as a 'black box' with limited user access to and control of build parameters, making post manufacturing certification and qualification challenging.

AM alloy fabrication processes in the most general sense employ directed energy (e.g., laser or electron beam) to bind/fuse feedstock materials (e.g., powder, rod, or sheet) to produce a predetermined geometric form. The selection and variation of the energy and build parameters offer flexibility in the product form and engender unique microstructures and defects or flaws that are unlike those found with other fabrication approaches. This becomes more significant under nonideal fabrication conditions, whereby defects such as porosity, lack of fusion voids (LOF; layer and cross-layer), and microcracking may be commonplace. LOF voids indicate poor bonding between the AM layers, and like microcracking, affect the tensile properties and fatigue life of the AM material [1]. The presence of larger pores can act as stress concentrators and serve as potential crack initiation sites. Full density alloys are required for high tensile or high torsional stress applications, such as those experienced by first line military parts, to minimize part failure during service [2].

The intentional seeding of defects in specimens should be a common practice for material quality assurance, nondestructive testing (NDT) guidelines, and obtaining mechanical properties for performance and safety standards [3]. One key criterion is that the seeding process must accurately produce the natural flaws that are known to occur from the actual fabrication process [4]. The ideal defect may be created through the modification of fabrication parameters in a systematic way, as opposed to artificial defects that may be produced via saw cuts or machined slots. The challenge with artificial discontinuities (side-drilled holes or flat-bottomed holes) is that the size, distribution, and morphology of the defect are not representative of naturally occurring defects [4].

A natural defect is more representative of a real AM part and is likely to produce a more realistic measurable change in material properties. The inherent flexibility in the AM processes is ideal for intentionally seeding defects into materials in a very controlled manner. In particular, laser additive manufacturing (LAM) methods (i.e., laser sintering, laser melting, or laser consolidation) employ focused laser energy to fuse powder feedstock together (or to an existing substrate) in a layer-by-layer manner to fabricate a high-density material. Through the variation of laser power and feedstock parameters, LAM processes may be employed to create defects and porosity between layers in alloys. For LAM systems, defects may be intentionally introduced by lowering the laser pulse energy, decreasing the pulse duration, increasing the laser scan speed, reducing the powder feed rate, or creating delamination by increasing the laser step-over distance between passes.

The principal concerns with LAM materials are the low surface quality (requires finish machining), the highly variable residual stresses, and that the maximum density achieved is typically ~98–99 % [5]. It is the evaluation of the latter concern that is the focus of this article. The measurement of bulk density is a versatile and effective method for quantifying the totality of the defects and quality of AM materials and for comparing the parts to other manufacturing approaches (e.g., casting and forming). There are a

variety of techniques for measuring the density in alloys. Slotwinski, Garboczi, and Heberstreit [6] employed the Archimedes' principle, a mass/volume approach, and X-ray computed tomography (XRCT) to examine porosity in cobalt-chrome (CoCr) parts made using a laser sintering AM system. Porosity results for each approach were similar and showed local variability of the porosity in each specimen. Spierings, Schneider, and Eggenberger [7] investigated the accuracy for Archimedes' method, microscopic analysis of cross sections, and XRCT for measuring density of 316L stainless steels fabricated using AM. The mean difference between the density values for a single specimen determined using a method based on Archimedes' principle was 0.13 ± 0.01 % for acetone, compared to 0.36 ± 0.08 % for water [7]. While not statistically significant, Archimedes' principle was an improvement on the results using the other two techniques.

Relative to the AM process monitoring, there is relatively little research dedicated to NDT for certification and qualification AM materials and parts [8]. Waller et al. [9] had identified the lack of suitable NDT techniques to detect AM defects as one of the most significant challenges to the acceptance of parts made through the AM process. There is a gap in knowledge related to the defect type, effect of defects, and the detectability limits for conventional and advancing approaches. The characterization of the size, geometry, and distribution of defects in AM materials is the driving force for the development of new NDT techniques. XRCT, radiographic testing (RT), and ultrasonic testing (UT) were identified as the more promising NDT methods for the characterization of internal defects [8,9]. XRCT has the capacity to image and distinguish defects in alloy specimens including density variation, pores, voids, and cracking. It enables the quantification of the size, morphology, frequency, and distribution of the defects as small as 10 μm (depending on instrument, analysis approach, and material size/geometry) via a sphere equivalent diameter (or similar) algorithm [10]. Although XRCT has the capacity to image the interior of specimens or parts and presents the data as a three-dimensional rendering, it is not portable, it is slow, and requires specimen preparation (resolution is affected by material thickness/size)—so it is not truly an NDT method. UT methods may also require surface preparation depending on the initial surface quality. RT and UT are portable, faster, and less expensive than CT. Research into RT is needed to determine its capacity to resolve micron-sized (<200 um) defects. Researchers have identified relationships between UT signals (e.g., pulse-echo, through-transmission, and immersion) and porosity [2,11]. Slotwinski, Garboczi, and Heberstreit [6] had described a linear relationship between the UT pulse-echo velocity and the degree of porosity down to (~ 0.5 %) porosity.

This study investigates the capacity for conventional portable NDT technologies to identify and classify defects that were intentionally seeded in 300M steel specimens fabricated using LAM processes. The goals were to assess LAM for intentionally seeding defects in LAM materials, determine the precision of several approaches for measuring density, and assess the limitations of traditional NDT techniques.

Test Methods

REFERENCE SPECIMENS

Well-characterized reference specimens with variations in density/porosity were required to identify correlations between NDT measurements and material defects. Specimens were produced using spherical, gas atomized, 300M steel powders. The 300M powder had a particle size range of 16–45 μm with the nominal chemical composition shown in **Table 1**.

TABLE 1

Nominal chemical compositions of 300M steel powders (wt. %).

C	Ni	Cr	Si	Mn	Mo	V	Fe
0.387	1.98	0.84	1.64	0.86	0.43	0.08	Bal.

Specimens were produced using the proprietary directed energy or blown powder laser consolidation (LC) system that was developed by the National Research Council of Canada (NRCC, Ottawa, Canada) [1,12]. The LC system employed a 500 W Lasag neodymium-doped yttrium aluminum garnet laser coupled with a fiber-optic processing head that operated in a pulse mode with an average power in the range of 200–250 W (LASAG, Belp, Switzerland). A Sultz-Metco 9 MP powder feeder was used to simultaneously deliver 300M powder into the melt pool through a nozzle at a powder feed rate in a range of 8–9 g/min (Oerlikon Metco, Pfäffikon, Switzerland). The software enabled variation of all laser settings and build parameters, thus enabling the fabrication of materials with unique microstructures and different volume fractions of defects. A pictorial representation of the build path is shown in Fig. 1. The scan direction was not rotated for subsequent layers in the build.

Several 300M steel AM specimens were produced with target densities between 99–95 % (or 1–5 % defects), as shown in Table 2. Specimens were designed to be sufficiently large to avoid edge effects from magnetic-based NDT techniques and to provide extractable regions for microstructural analysis. The approach used for introducing the defects was to start with a full density build and then change the hatch speed and spacing with the goal of producing evenly distributed defects throughout. Six specimens were made with target bulk density from 99 to 95 % (1 to 5 % defects). Specimens D and E were made with a ~1-mm-thick higher density outer layer to seal the surface against potential liquid entrapment. The full-density outer layer on these two specimens was fabricated using optimized AM processing parameters. The outer layer of Specimens A, B, C, and F displayed exposed surface porosity on all sides.

All LAM specimens were cut from the substrate and then subjected to austenitizing at 871°C followed by oil quenching, double tempering at 302°C, and air cooling. After the heat treatment, all LC 300M specimens were surface ground and then electrical discharge machined to the final dimensions of 150 mm (x-direction) by 60 mm (y-direction) and either 3-mm (specimens A, B, C, and F) or 4.5-mm (specimens D and E) thick

FIG. 1

Pictorial representation of the orientation of the build path.

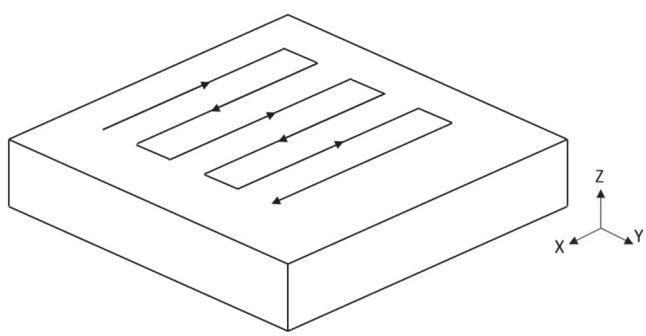

TABLE 2

Target and average measured densities for 300M specimens that were determined using laser metrology, coordinate measuring machine (CMM), and optical microscopy (averaged across three planes).

			Direct Density Measurements					
			Metrology		CMM		Microscopy	
Reference Specimen	Target Density, %	Target Defects, %	Density, %	St. Dev., %	Density, %	St. Dev., %	Density, %	St. Dev., %
A	99	1	98.5 %	0.6 %	97.5 %	1.1 %	98.2 %	0.6 %
B	99	1	98.1 %	0.3 %	97.8 %	1.2 %	98.4 %	0.5 %
C	97.5	2.5	99.9 %	1.2 %	95.8 %	1.0 %	94.5 %	2.5 %
D[a]	97.5	2.5	97.2 %	0.6 %	96.2 %	0.4 %	94.9 %	2.4 %
E[a]	96	4	96.8 %	0.1 %	95.6 %	0.4 %	93.5 %	1.5 %
F	96	4	97.7 %	0.9 %	93.3 %	0.8 %	91.3 %	3.4 %

Note: [a] Specimens D and E were built with a ~1-mm-thick full density outer layer.

(z-direction). The thinner specimens contained exposed defects, while the thicker specimens had the full density outer-layer. A 300M wrought specimen was heat treated and machined to final dimensions (150 mm by 60 mm by 3 mm) using the same procedures used in making LAM specimens.

MICROSCOPIC IMAGING

The microstructure and relative variation in defects were then observed with optical microscopy (OM) and scanning electron microscopy (SEM). Portions of the LAM specimens were sectioned and polished to view the microstructures both parallel and perpendicular to the build or z-direction. After polishing the surfaces to a 0.25-μm finish, the surfaces were etched with 2 % nitric acid.

DENSITY MEASUREMENTS

Direct Density Methods

The methodology used to seed defects was expected to produce local variations in the plane perpendicular to the build direction. The part densities were calculated from the mass measured with an analytical balance and the volume measured with two surface dimension measurement approaches. A metrology system (Nikon MMDx 3D laser scanner [Nikon, Tokyo, Japan]) and a Mitutoyo coordinate measuring machine (CMM, model #BHN715 [Mitutoyo, Kawasaki, Japan]) were used to generate three-dimensional models of the specimens and to calculate volume.

Optical Microscopy

OM software was employed to measure the relative percentage of defects (voids, pores, cracking, and inclusions) on a polished specimen surface. The software quantified the contrast between light (full-density) and dark (defect) regions of OM images. Cross sections were taken in three orthogonal planes and polished to a 0.25-μm finish. Measurements were made at several locations, and specimens were reground and polished five times to provide measurement of density variation with depth.

Archimedes' Principle

The relative density of fabricated specimens was determined using an approach based on the Archimedes' principle. Archimedes' principle states that the buoyant force experienced

by a submerged object is directed upward and is equivalent to the weight (or force) of the liquid displaced by the object. The fundamental Archimedes' equation may be simplified such that the density of the object can be calculated independent of a change in liquid volume [13]. The density of an object (ρ_{obj}) can be calculated from the density of the liquid (ρ_{liq}), the mass of the object in air (m_{obj}), and the equivalent mass increase of the system when the specimen is submerged (m_{liq}) [2].

$$\rho_{obj} = \rho_{liq} \cdot \frac{m_{obj}}{(m_{obj} - m_{liq})} \quad (1)$$

The mass of each specimen was measured in air (m_{obj}) using an analytical balance. A test apparatus, shown in **Fig. 2**, was designed and constructed based on the Archimedes' principle [13]. **Fig. 2** shows a beaker filled with a liquid (i.e., deionized water and <0.05 vol. % surfactant) on the balance and a wired specimen supported from a stand. The balance was tared prior to adding the specimen. The specimen was then placed into the support and fully submerged close to the free surface to determine m_{liq}. It was also assumed that the wire specimen support (AWG32 copper wire) would have a negligible effect on density calculations because of its low mass and size relative to the test specimen [13,14]. Any air bubbles adhering to the specimen were carefully removed using a thin copper wire to avoid liquid removal from the beaker.

The density of the working liquid (ρ_{liq}) was measured with a hydrometer and the density of each specimen (p_{obj}) was calculated using Eq 1. To account for the buoyancy of the test pieces in air, the addition of a correction factor based on the density of air was included [6,7]. Relative density values were calibrated with respect to a full-density wrought 300M specimen (7.77 g/cm^3) measured using the same approach. Masses were measured to four significant digits, with the measurement of (ρ_{liq}) representing the most significant source of error. Measurements were repeated five times and no outliers were identified using ASTM E178-08, *Standard Practice for Dealing with Outlying Observations*, and Dixon's Q test with a significance level of 0.05 [15]. The Q test is dimensionless and is only compared to the reference values provided in ASTM E178 as a rejection criterion for outlier examination [16]. The significance level is 0.05 or 5 %, which is equivalent to a 95 % confidence interval.

FIG. 2

Test apparatus for measurement of bulk density using Archimedes' principle.

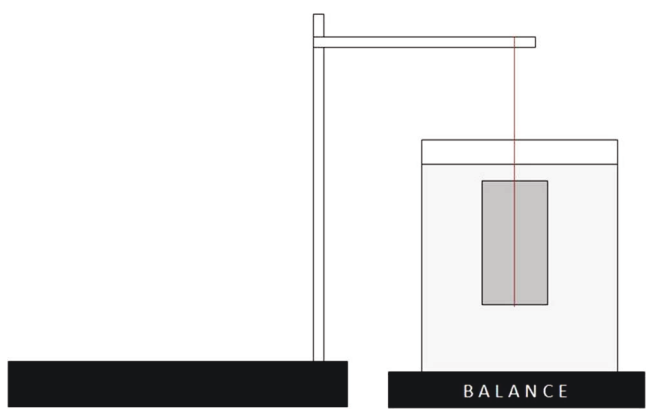

In addition to deionized water, acetone and n-hexane were also used as working liquids to examine the effects of surface tension and volatility on measurement accuracy. Water with a small quantity of added surfactant (approximately 0.05 volume %) was used to take initial measurements. The small quantity of added surfactant was assumed to not change the density of the working liquid significantly [13]. Under laboratory conditions, the density of the water was estimated to be 0.9989 g/cm^3 [17]. Acetone and n-hexane were chosen as suitable working liquids due to their low surface tension, thereby making them better wetting agents. However, acetone caused problems when trying to obtain precise measurements because of its high volatility. The liquid density was measured immediately before testing using a set of American Petroleum Institute hydrometers.

NON-DESTRUCTIVE CHARACTERIZATION

Radiographic Testing

Gamma RT was used to measure the density threshold at which defects may be detected in the LAM specimens. Using Kodak MX125 film (Kodak, Rochester, NY), specimens were exposed to an iridium-192 gamma radiation source with a working distance of approximately 50.8 cm. The films were developed to achieve a reading of 2.45 on a densitometer, indicating an appropriate gray balance for viewing traditional defects.

Ultrasonic Testing

UT was performed with an EPOCH 1000i ultrasonic flaw detector (Olympus, Tokyo, Japan) using a 6-mm, 5-MHz longitudinal magnetic hold down contact longitudinal probe (Olympus M1057). It was expected that the smaller wavelength of 5 MHz would have a higher sensitivity to the microstructural defects relative to low frequency probes. Tests were conducted with a 100-V spiked pulse echo and a 50-Ω damping element. To minimize errors, a constant voltage and volume of coupling gel was used for each test.

Results and Discussion

MACROSTRUCTURE

300M LAM specimens with 99 % density at the surface (Specimen A) did not exhibit any visible surface defects. The surface exhibited a texture, likely from surface grinding (Fig. 3).

FIG. 3

Photograph of the surface of Specimen A.

MICROSTRUCTURE

Heat-treated 300M LAM specimens appear to exhibit a lath tempered martensite (possibly bainite) grain structure (Fig. 4a). They contained isolated defects, both pore (Fig. 4b) and LOF voids (Fig. 5b). In order to preserve the integrity of the specimens for NDT, hardness tests were not performed on each specimen to verify microstructures. Hardness tests on similar specimens revealed Vickers hardness values of ~550 ± 50. Pores were spherical and varied in size from 5 to 50 μm (Fig. 4b). They appeared to be randomly distributed throughout each specimen and at similar concentrations. The pores, common to most AM techniques, likely represent residual gases (typically argon, nitrogen, or trace oxygen) trapped in the powder during manufacturing and then incorporated during laser melting and subsequent solidification. Studies have traced these pores back to the atmosphere in which the powders are atomized [10].

300M LAM specimens show distinct LOF defects (Fig. 5) that propagate in the z-direction of the build. The number and size increase as the net density decreases. This was likely from the process used to introduce the defects. SEM images show LOF defects in Specimen E were from 500–1,000 μm in length. A typical LOF void is shown in Fig. 5a. Fig. 5b clearly shows the unmelted or unconsolidated powder (from 10–50-μm diameters) located within one of the LOF voids. The size of the voids was much larger than the gas bubble porosity (5–50 μm).

FIG. 4

Optical microscope (OM) images showing the lath tempered martensite/bainite grain structure that was typical of all specimens (a) without and (b) with a pore and microcracking.

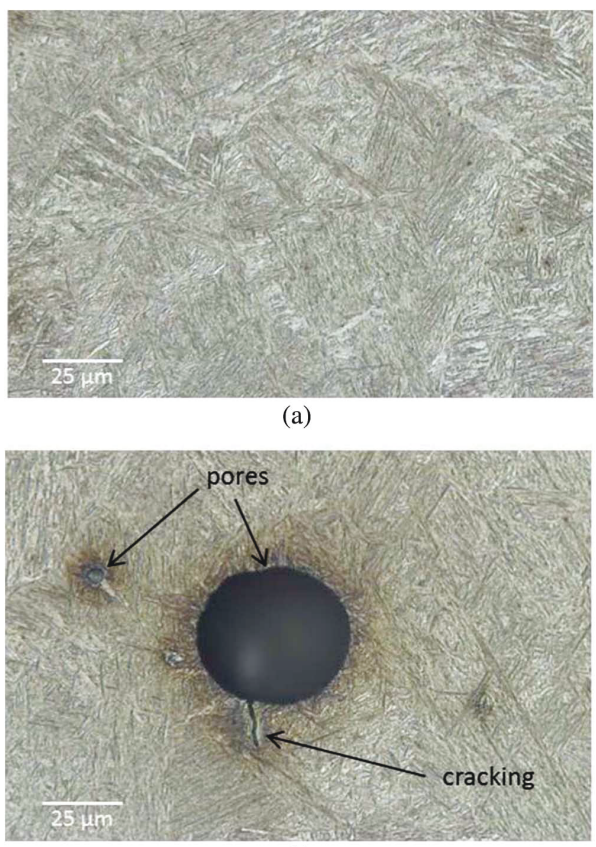

FIG. 5

SEM images showing typical (a) lack of fusion void and (b) close-up of the unconsolidated powder granules found in Specimen E.

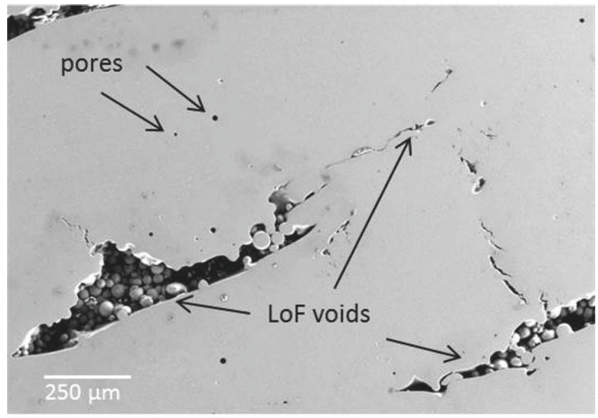

(a)

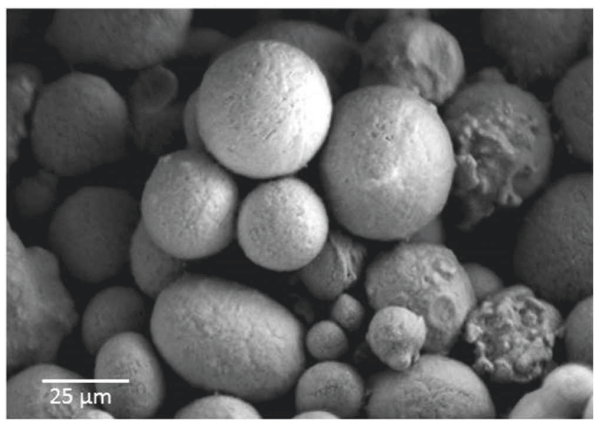

(b)

LOF voids are common with directed energy deposition techniques and manifest when individual powder granules are not melted or are only partially melted and form irregular and jagged void spaces in the build. LOF voids may be intentionally introduced into a specimen by lowering the laser pulse energy, decreasing the pulse duration, increasing the laser scan speed, reducing the powder feed rate, or creating delamination by increasing the laser step-over distance between passes.

DENSITY MEASUREMENTS

Direct Density Methods

Bulk density measurements were made using an analytical balance and direct dimensioning approaches. Laser metrology and CMM measurement were found to provide a consistent estimate of density with standard deviations ranging from 0.2–1.0 % and 0.5–1.1 %, respectively (Table 2).

Optical Microscopy

OM images were collected as a function of depth and in three orthogonal directions for all specimens. Fig. 6 shows OM images for Specimen A that were typical for both ~99 % density specimens at the different depths. Images showed what appeared to be grain

FIG. 6 OM images showing typical microstructure for Specimen A with 99 % density.

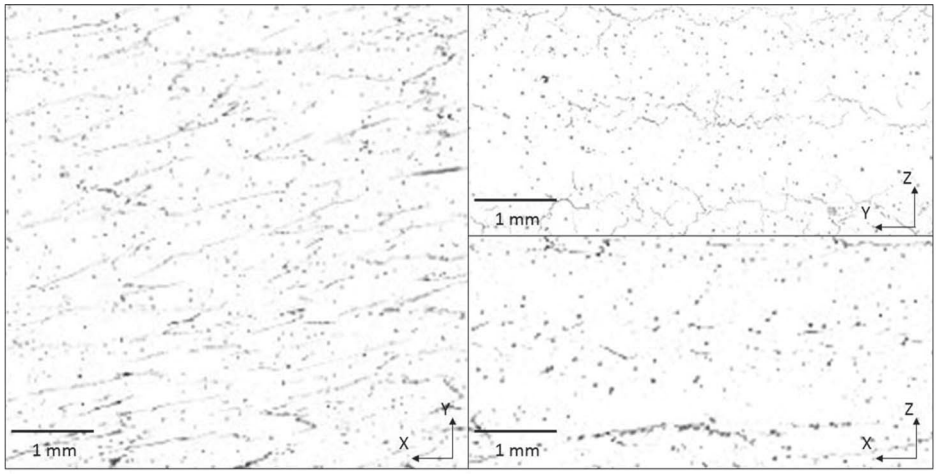

boundaries and distributed spherical porosity. OM images at lower densities showed lack of fusion voids with preferential void localization at specific layers through the thickness of each specimen. In general, lack of fusion voids were elongated and possibly interconnected. This localization is a consequence of the change in the hatch speed and spacing used to produce the distributed defects throughout each specimen.

OM density measurements were made as a function of depth using contrast imaging. Results are shown in **Fig. 7**. Greater fluctuations in pore fraction by area in the XY plane with depth may indicate pore propagation in the z-direction, assuming consistent pore width (y-direction) in adjacent layers of the build, similar to what is seen with selective melting techniques [15]. This means that existing pores would have a tendency to affect powder deposition in subsequent layers. This indicates that the defects were successfully introduced by modification of in-layer build parameters (i.e., hatch spacing or scan speed).

The area percentage of defects as a function of depth in the XY, XZ, and YZ planes are shown in **Table 3**. As expected, there appears to be a greater degree of void localization in the higher porosity specimens, where wider fluctuations in the pore area exist over small depth changes. In general, average OM measurements (**Table 3**) were found to be less precise than metrology and CMM with a standard deviation range of 0.6–3.0 %. The large deviation in measurements suggest that it is advisable to avoid OM measurements to obtain density values. A better technique is needed to calculate the standard deviation as the variation likely represents changes to the intentional void fraction at each layer. OM does provide important information pertaining to the location and morphology of voids and porosity.

Archimedes' Principle

Archimedes' principle was tested on the as-received specimens before sectioning for OM. The results are shown in **Table 4** for several different media. The more common approach, with deionized water as the displacement liquid, resulted in average values that were within 0.5 % of the target values (**Table 4**) and standard deviations ranging from 0.1–0.3 %. While most air bubbles were removed, the occurrence of smaller bubbles would affect repeatability.

Using acetone as the displacement liquid resulted in a decrease in average values and an increase in the standard deviation range to 0.2–0.4 %. This is believed to be due to the

FIG. 7 OM through-thickness porosity measurements as a function of depth and plane in each of the six reference specimens.

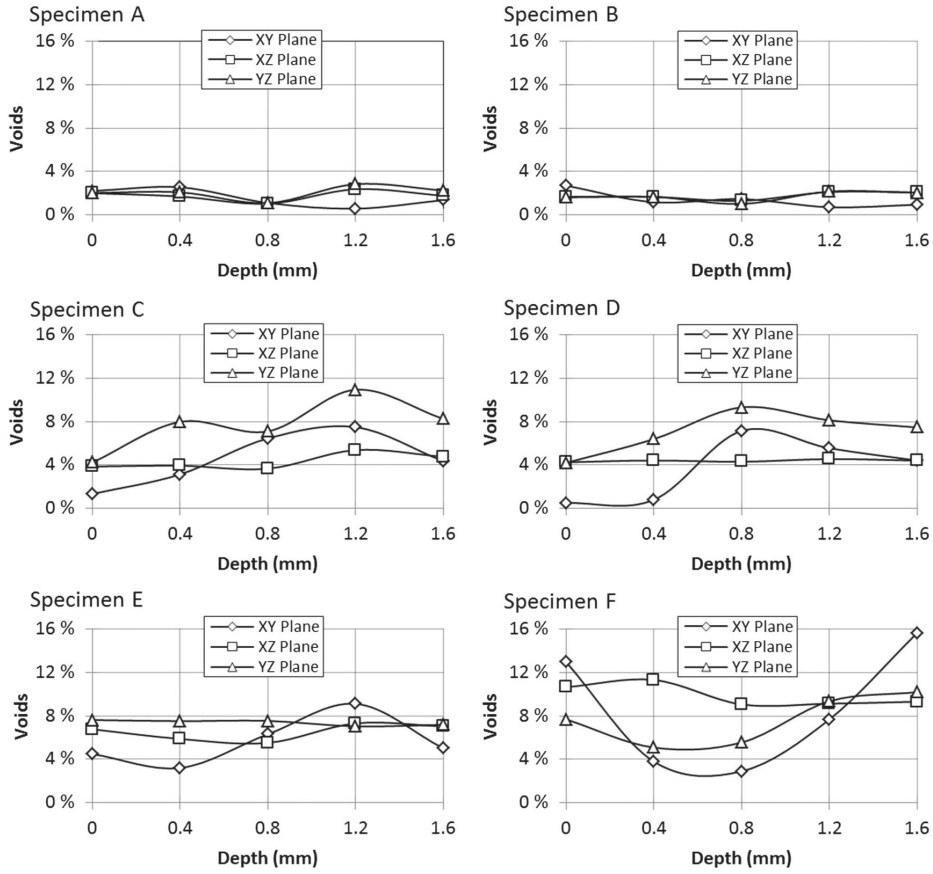

TABLE 3

Average measured densities for 300M specimens determined from optical microscopy as a function of three perpendicular planes.

			XY Plane		XZ Plane		YZ Plane	
Reference Specimen	Target Density, %	Target Defects, %	Density, %	St. Dev., %	Density, %	St. Dev., %	Density, %	St. Dev., %
A	99	1	98.5 %	0.6 %	97.5 %	1.1 %	99.0 %	0.2 %
B	99	1	98.1 %	0.3 %	97.8 %	1.2 %	99.2 %	0.1 %
C	97.5	2.5	99.9 %	1.2 %	95.8 %	1.0 %	97.5 %	0.0 %
D[a]	97.5	2.5	97.2 %	0.6 %	96.2 %	0.4 %	97.1 %	0.1 %
E[a]	96	4	96.8 %	0.1 %	95.6 %	0.4 %	95.8 %	0.1 %
F	96	4	97.7 %	0.9 %	93.3 %	0.8 %	95.9 %	0.2 %

Note: [a] Specimens D and E were built with a ~1-mm-thick full density outer layer.

high volatility of acetone. N-hexane was tested because it had low volatility and low surface tension (similar to acetone). Average values with n-hexane were more consistent with target values (Table 4) and had the lowest standard deviation range of 0.0–0.2 % of all media tested—only marginally different from water.

TABLE 4
Target and measured densities for 300M specimens using Archimedes' principle.

			Deionized Water		Acetone		n-Hexane	
Reference Specimen	Target Density (%)	Target Defects (%)	Density (%)	St. Dev. (%)	Density (%)	St. Dev. (%)	Density (%)	St. Dev. (%)
A	99	1	98.9 %	0.2 %	98.4 %	0.4 %	99.0 %	0.2 %
B	99	1	99.0 %	0.1 %	98.2 %	0.3 %	99.2 %	0.1 %
C	97.5	2.5	97.0 %	0.1 %	97.0 %	0.2 %	97.5 %	0.0 %
D[a]	97.5	2.5	97.0 %	0.1 %	96.8 %	0.2 %	97.1 %	0.1 %
E[a]	96	4	95.7 %	0.1 %	94.8 %	0.2 %	95.8 %	0.1 %
F	96	4	95.5 %	0.4 %	95.2 %	0.4 %	95.9 %	0.2 %

Note: [a] Specimens D and E were built with a 1-mm-thick full density outer layer.

The Archimedes' method evaluates the bulk porosity of the specimen rather than localization effects while giving a more accurate measurement for larger specimens over smaller specimens. The repeatability of the Archimedes method with n-hexane was an improvement over acetone, but comparable to deionized water. The variability in density standard deviation ranges was 0.0–0.2 % for n-hexane compared to 0.1–0.3 % for water. To potentially diminish the effects of the volatility of the liquid and the surface tension, it may be beneficial to conduct the tests at reduced temperature to lower the surface tension and vapor pressure.

NON-DESTRUCTIVE TESTING

Liquid penetrant testing failed to discern any noticeable variations between the specimens of varying density. Magnetic particle testing showed unique electromagnetic patterns. Results require more interpretation but likely relate to the build pattern or magnetic structure of the alloy.

Radiographic Testing

Gamma RT was performed on all six specimens (see Fig. 8). The resulting radiographs clearly showed texture in the lower density specimens (Fig. 8b and c) that was not apparent in the high-density specimen (Fig. 8a). This indicates that the detection threshold for porosity/voids is likely between 1.0 % and 2.5 %, assuming a uniform distribution through the specimen. This may also be impacted by a slight variation (<0.1 mm) in specimen thickness. The results reaffirm that the pores appear primarily unidirectional in the x-direction.

Ultrasonic Testing

UT revealed some interesting features in the backwall reflections (Fig. 9). The wrought specimen (Fig. 9a) clearly displays the first seventeen backwall reflections, indicating very thorough ultrasonic transmission because of the lack of defects. In contrast, the introduction of defects within the 99 % density LAM specimen (Specimen A, Fig. 9b) creates a large quantity of background noise around the first backwall reflection and completely dampens all subsequent reflections. This is believed to be due to ultrasonic attenuation from the voids, but it may also represent the effect of residual stress fields in the specimen. Stress-relieving the specimen is expected to provide clarification.

At a frequency of 5 MHz, defects that were smaller than 120 μm (using a typical detectability limit of 10 % of the wavelength) should be undetectable. Therefore, the

FIG. 8

Radiographs of (a) Specimen A with 99 % density, (b) Specimen C with 97.5 % density, and (c) Specimen E with 95.8 % density.

(a)

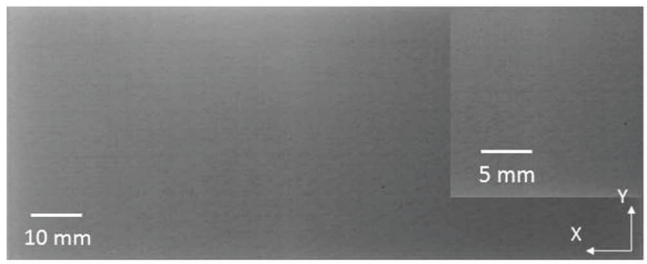

(b)

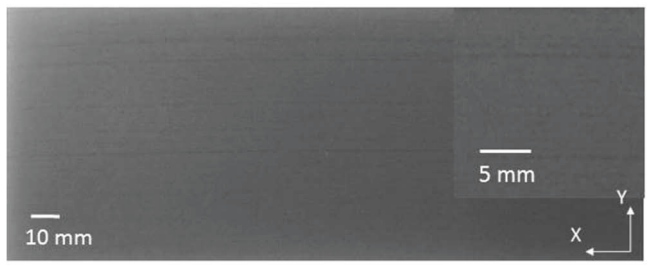

(c)

5 to 50-μm-diameter spherical pores should be undetectable. The largest of the LOF (from 500–1,000 μm) defects may be discernible. Given that the 300M LAM and 300M wrought specimen were subjected to the same heat treatment, the differences in attenuation were not believed to be caused by differences in microstructure.

Fig. 10 shows repeat measurements of ultrasonic gain required to boost the backwall reflection to 80 % of full screen height (FSH). This method was utilized because of the lack of backwall reflection in the AM specimens, and, therefore, the lack of data available for absolute attenuation measurement. The backwall reflections for each specimen showed a clear correlation between density and echo amplitude. The average gain required to reach 80 % FSH on the back wall reflection for the 3-mm-thick specimens was 15 dB/mm for the 99 % density specimens, 17.5 dB/mm for the 97.5 % specimens, and 20 dB/mm for the 96 % specimens. For the 4.5-mm-thick specimens (1.25-mm overlayers), values of 12 dB/mm and 17 dB/mm were recorded for the 97.1 % and 96 % specimens, respectively. The results are similar to those measured on the wrought specimens.

The distribution was promising for using ultrasonic gain as a qualification mechanism for measuring density in LAM components. There exists a clear upward trend of increasing gain with an increase in porosity for similarly-sized specimens. There was also a decrease in gain with an increase in specimen thickness. It is unclear whether the lower

FIG. 9

Traces of the ultrasonic transmission backwall reflections of (a) wrought 300M steel and (b) Specimen A with 99 % density.

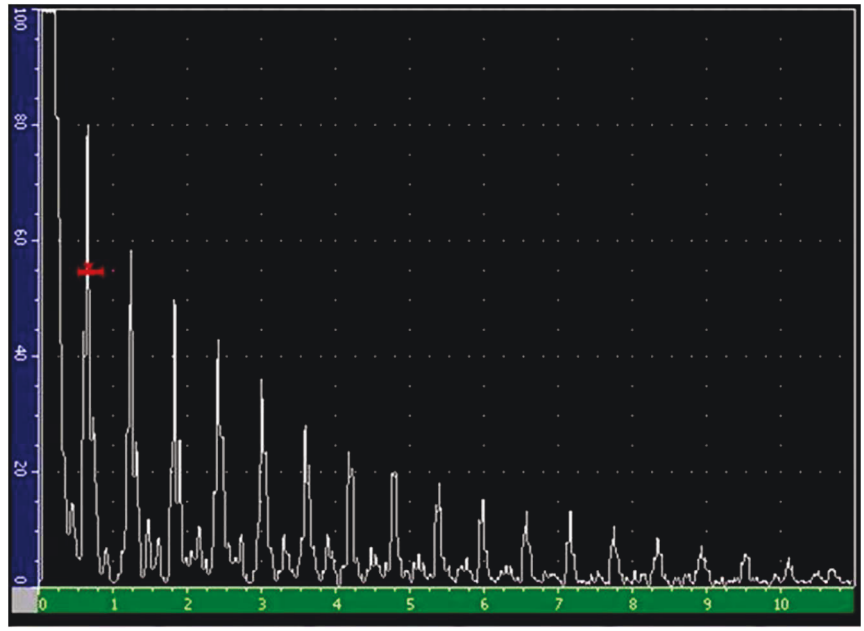

(a)

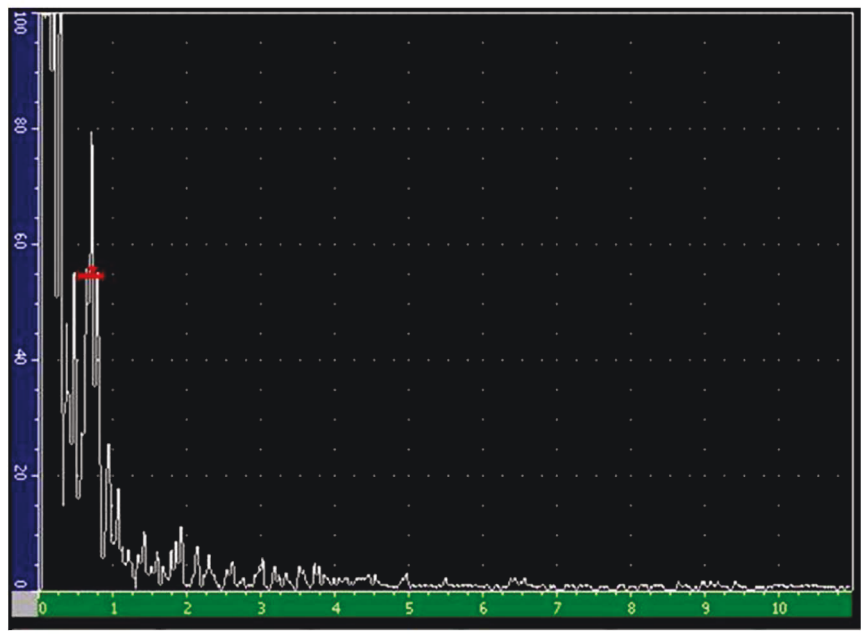

(b)

apparent attenuation of the thicker specimens arose from the presence of the full-density outer layers or from diffraction effects. The results are still preliminary. Future work on additional specimens over the 100–98 % density range with different thicknesses is expected to provide clarification.

FIG. 10

Correlation between standardized ultrasonic gain at 80 % of FSH and density as determined using Archimedes' principle and n-hexane as the displacement liquid.

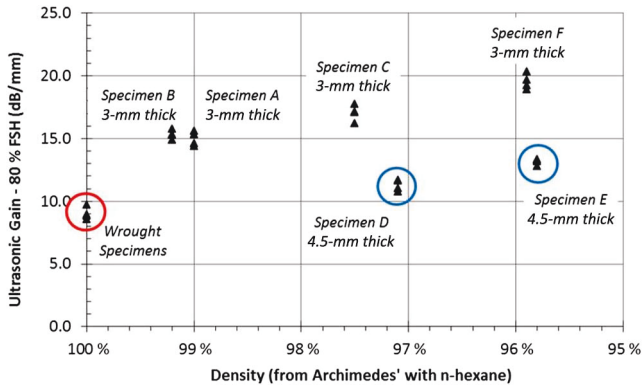

Conclusions

This article compared the methods for determining density and the capacity for conventional NDT technologies to identify defects that were intentionally seeded in 300M steel specimens that are fabricated using a LAM process. The main conclusions are as follows:

(1) The densification of 300M steel specimens was controlled through modification of LAM fabrication parameters. Specimens appeared to have a threshold limit of porosity. LOF voids increased with an increase in the hatch speed or hatch spacing.
(2) The Archimedes' principle was shown to have a mean difference between density values of 0.1 ± 0.1 % when using n-hexane as the displacement liquid. This method is easier, faster, and more economic than the other approaches evaluated here.
(3) In terms of conventional NDT, the detection threshold for the 500–1000 μm defects using the RT approach was between 1 % and 2.5 %, assuming a uniform distribution through the specimen. UT results identified ultrasonic gain as a promising characteristic for the estimation of through-thickness density in LAM components.
(4) Future work will examine several specimens over the 100–98 % density range. In addition, additional specimens will be investigated with phased-array UT and magnetic Barkhausen noise analysis. Mechanical testing will examine the effects of microstructure and defects on overall material performance.

ACKNOWLEDGMENTS

The authors would like to thank Dr. Lijue Xue of the National Research Council of Canada for fabrication of specimens and Mr. Kyle Avery, Mrs. Nancy Hervé, and Mr. Tom Lemczyk from Defence Research and Development Canada, Atlantic Research Centre, for their assistance in preparing and testing specimens.

References

[1] Xue, L. and Islam, M. U., "Free-Form Laser Consolidation for Producing Metallurgically Sound and Functional Components," *J. Laser Appl.*, Vol. 12, 2000, pp. 160–165, https://doi.org/10.2351/1.521927

[2] Slotwinski, J. A. and Garboczi, E. J., "Porosity of Additive Manufacturing Parts for Process Monitoring," presented at the *40th Review of Progress in Quantitative Non-Destructive Evaluation*, Baltimore, MD, July 22–26, 2013, pp. 1581–1589.
[3] Consonni, M., Howse, D., Wee, C. F., and Schneider, C., "Production of Joints Welded with Realistic Defects," *Weld. Int.*, Vol. 28, No. 7, 2013, pp. 535–546, https://doi.org/10.1080/09507116.2012.753263
[4] Crutzen, S., Lemaitre, P., and Iacono, I., "Realistic Defects Suitable for ISI (in Service Inspection) Capability Evaluation and Qualification," presented at the *14th International Conference on NDE in the Nuclear and Pressure Vessel Industries*, Stockholm, Sweden, Sep. 24–26, 1996, ASM International, Materials Park, OH, pp. 153–163
[5] Yasa, E. and Kruth, J.-P., "Microstructural Investigation of Selective Laser Melting 316L Stainless Steel Parts Exposed to Laser Re-melting," *Procedia Eng.*, Vol. 19, 2011, pp. 389–395, https://doi.org/10.1016/j.proeng.2011.11.130
[6] Slotwinski, J. A., Garboczi, E. J., and Heberstreit, K. M., "Porosity Measurements and Analysis for Metal Additive Manufacturing Process Control," *J. Res. Nat. Inst. Stand. Technol.*, Vol. 119, 2014, pp. 494–528, https://doi.org/10.6028/jres.119.019
[7] Spierings, A. B., Schneider, M., and Eggenberger, R., "Comparison of Density Measurement Techniques for Additive Manufactured Metallic Parts," *Rapid Prototyping J.*, Vol. 17, No. 5, 2011, pp. 380–386, https://doi.org/10.1108/13552541111156504
[8] Sharratt, B., "Non-destructive Techniques and Technologies for Qualification of Additive Manufactured Parts and Processes: A Literature Review," *Defence Research and Development Canada Contract Report DRDC-RDDC-2015-C035*, Sharratt Research & Consulting Inc, Victoria, Canada, 2015, 47p.
[9] Waller, J. M., Parker, B. H., Hodges, K. L., Burke, E. R., and Walker, J. L., "Nondestructive Evaluation of Additive Manufacturing: State-of-the-Discipline Report," *NASA Technical Memorandum 2014–218560*, National Aeronautics and Space Administration, Washington, DC, 2014, 20140016447.
[10] Rao, S., Cunningham, R., Ozturk, T., and Rollett, A. D., "Measurement and Analysis of Porosity in Al-10Si-1Mg Components Additively Manufactured by Selective Laser Melting," *Mater. Perform. Charact.*, Vol. 5, No. 5, 2016, pp. 701–716.
[11] Boccaccini, D. N. and Boccaccini, A. R., "Dependence of Ultrasonic Velocity on Porosity and Pore Shape in Sintered Materials," *J. Nondestr. Eval.*, Vol. 16, No. 4, 1997, pp. 187–192, https://doi.org/10.1023/A:1021891813782
[12] Xue, L., Li, Y., and Wang, S., "Direct Manufacturing of Net-Shape Functional Components/Test-pieces for Aerospace, Automotive and Other Applications," *J. Laser Appl.*, Vol. 23, No. 4, 2011, pp. 042004-1–042004-8, https://doi.org/10.2351/1.3622200
[13] ASTM B311-08, *Standard Test Method for Density of Powder Metallurgy (PM) Materials Containing Less Than Two Percent Porosity*, ASTM International, West Conshohocken, PA, 2008, www.astm.org
[14] ASTM B962-08, *Standard Test Method for Density of Compacted or Sintered Powder Metallurgy (PM) Products Using Archimedes' Principle*, ASTM International, West Conshohocken, PA, 2008, www.astm.org
[15] Bauereiβ, A., Scharowsky, T., and Körner, C., "Defect Generation and Propagation Mechanism during Additive Manufacturing by Selective Beam Melting," *J. Mater. Process. Technol.*, Vol. 214, No. 11, 2014, pp. 2522–2528, https://doi.org/10.1016/j.jmatprotec.2014.05.002
[16] ASTM E178-08, *Standard Practice for Dealing with Outlying Observations*, ASTM International, West Conshohocken, PA, 2008, www.astm.org
[17] Taylor, J. K. and Oppermann, H. V., *Handbook for the Quality Assurance of Metrological Measurements*, NBS Handbook 145, National Bureau of Standards, Gaithersburg, MD, 1986, 326p.

DOCUMENT CONTROL DATA

*Security markings for the title, authors, abstract and keywords must be entered when the document is sensitive

1. ORIGINATOR (Name and address of the organization preparing the document. A DRDC Centre sponsoring a contractor's report, or tasking agency, is entered in Section 8.)

DRDC – Atlantic Research Centre
Defence Research and Development Canada
9 Grove Street
P.O. Box 1012
Dartmouth, Nova Scotia B2Y 3Z7
Canada

2a. SECURITY MARKING (Overall security marking of the document including special supplemental markings if applicable.)

CAN UNCLASSIFIED

2b. CONTROLLED GOODS

NON-CONTROLLED GOODS
DMC A

3. TITLE (The document title and sub-title as indicated on the title page.)

Analysis of Seeded Defects in Laser Additive Manufactured 300 M Steel

4. AUTHORS (Last name, followed by initials – ranks, titles, etc., not to be used)

Farrell, S. P.; Deering, J.

5. DATE OF PUBLICATION (Month and year of publication of document.)	6a. NO. OF PAGES (Total pages, including Annexes, excluding DCD, covering and verso pages.)	6b. NO. OF REFS (Total references cited.)
July 2018	16	17

7. DOCUMENT CATEGORY (e.g., Scientific Report, Contract Report, Scientific Letter.)

External Literature (P)

8. SPONSORING CENTRE (The name and address of the department project office or laboratory sponsoring the research and development.)

DRDC – Atlantic Research Centre
Defence Research and Development Canada
9 Grove Street
P.O. Box 1012
Dartmouth, Nova Scotia B2Y 3Z7
Canada

9a. PROJECT OR GRANT NO. (If appropriate, the applicable research and development project or grant number under which the document was written. Please specify whether project or grant.)	9b. CONTRACT NO. (If appropriate, the applicable number under which the document was written.)
01EB-4.4.1	

10a. DRDC PUBLICATION NUMBER (The official document number by which the document is identified by the originating activity. This number must be unique to this document.)	10b. OTHER DOCUMENT NO(s). (Any other numbers which may be assigned this document either by the originator or by the sponsor.)
DRDC-RDDC-2018-P104	

11a. FUTURE DISTRIBUTION WITHIN CANADA (Approval for further dissemination of the document. Security classification must also be considered.)

Public release

11b. FUTURE DISTRIBUTION OUTSIDE CANADA (Approval for further dissemination of the document. Security classification must also be considered.)

12. KEYWORDS, DESCRIPTORS or IDENTIFIERS (Use semi-colon as a delimiter.)

additive manufacturing, directed energy, selective laser melting, Archimedes' principle, density, defects, porosity, ultrasonic spectroscopy, radiographic testing

13. ABSTRACT/RÉSUMÉ (When available in the document, the French version of the abstract must be included here.)

This research activity was initiated to better assess the capacity for traditional nondestructive testing (NDT) approaches to ascertain the defects inherent to materials fabricated through a directed energy laser additive manufacturing (LAM) process. A methodology was developed to intentionally seed defects in 300M steel specimens through intermittent modification of fabrication parameters. Several 300M steel specimens were fabricated and the concentration of defects or bulk density was characterized using optical microscopy and variations of the Archimedes' principle. Specimens were then evaluated using NDT (radiographic testing, ultrasonic testing). Results show that by using n-hexane as the displacement liquid, the Archimedes' principle was found to have repeatability in density values of 0.1 ± 0.1 %. The results reveal the unique defects produced through the LAM process and the limitations for conventional NDT techniques to adequately detect defects in LAM materials. Ultrasonic testing was found to be a promising tool for assessing the LAM defect distribution. Future work will focus on LAM alloys with higher densities and relate microstructure and defects to overall material performance.